Desalination and Water Treatment
www.deswater.com
doi: 10.5004/dwt.2022.28135

249 (2022) 33–46
February

Antifouling polyethersulfone composite ultrafiltration membrane fabricated with SiO_2-g-PAA as additive and its application in oil-in-water emulsion

Jun Yin*, Xinan Cai, Bingshan Wang

School of Biological and Environmental Engineering, Jing de zhen University, Jing de zhen 333000, Jiangxi, China, email: yinminghan@163.com (J. Yin)

Received 21 March 2021; Accepted 2 January 2022

ABSTRACT

In order to reduce silica nanoparticles (SiO_2 NPs) agglomeration, improve the dispersity of SiO_2 NPs in the matrix of polyethersulfone (PES) composite membrane, the poly (acrylic acid) grafted SiO_2 NPs (SiO_2-g-PAA NPs) are beforehand synthesized via surface-initiated activators regenerated by electron transfer atom transfer radical polymerization (ARGET ATRP). PES/SiO_2-g-PAA organic-inorganic composite membranes are convenient fabricated by blending PES matrix with the as-synthesized SiO_2-g-PAA NPs via the non-solvent induced phase separation (NIPS) process. The attenuated total reflectance Fourier-transform infrared spectroscopy and surface scanning electron microscope (SEM) results confirm that the well dispersed SiO_2-g-PAA NPs tend to migrate toward the membrane top surfaces. As a result, the composite membrane exhibited the highest pure water flux and oil flux around 233.72 and 97.29 L/m²h, which equal to 3.6 times and 8.8 times of unmodified PES membrane respectively. The flux recovery rate increased from 45.74% to 77.12%, suggesting the fouling-resistance of the composite membranes was greatly improved. Furthermore, the SiO_2-g-PAA NPs exhibit excellent stability in the membrane matrix benefit from the interaction between PAA polymer chains and PES. In addition, the reactive PAA chains on the membrane surface provide a platform for further functionalization.

Keywords: Organic–inorganic composite membrane; Surface-initiated ARGET ATRP; Antifouling; SiO_2-g-PAA; Oil-in-water emulsion

1. Introduction

With the rapid development of industry, a large amount of oily wastewater are generated by many industrial processes [1,2], resulting in terrible environmental pollution. Hence, efficient advanced separation technologies must be developed to treating oily wastewater, especially surfactant-stabilized oil-in-water emulsion.

The application of membrane separation technology for treating oil-in-water emulsion has attracted considerable attention over the past decennia [3–7]. The advantages of membrane separation technology are that low energy requirement, easy to handle, negligible environmental pollution and works without addition of toxic chemicals. Some hydrophobic polymer materials, including polysulfone (PS), polyethersulfone (PES), polyvinylidene fluoride (PVDF) and polyacrylonitrile (PAN) were increasingly used to prepare microfiltration or ultrafiltration membranes [3–7]. Their extensive application was a result of outstanding physicochemical property and the excellent membrane-forming property. However, hydrophobic membrane materials are prone to suffer from serious foul because of adsorption and pore plugging by oil droplets, which results in a quick decline of permeation [4,6]. Accordingly, numerous approaches including physical blending, surface coating, surface grafting and chemical modification of membrane bulk material had been carried out to improve hydrophilicity of the polymeric membrane for addressing

* Corresponding author.

the membrane foul [8–16]. Masuelli et al. [15] prepared PVDF-g-(PGMAS-co-PEDMA) membranes which exhibited enhanced anti-fouling property via surface grafting. Chen et al. [16] synthesized CA-g-PAN membrane via chemical modification of membrane bulk material, the pure water flux of CA-g-PAN was almost 100 times of unmodified CA membrane, the flux recovery rate reached 100%, suggesting the fouling-resistance of the composite membranes was greatly enhanced. Compared to other modification methods, physical blending becoming a research hotspot benefit from its facile preparation procedure and can achieve three-dimensional modification [17–19]. The inchoate blending modification was to directly blend hydrophilic polymer with membrane matrix. Marchese et al. [17] used polyvinylpyrrolidone (PVP) as a hydrophilic additive, blending with PES to prepare composite membrane with improved permeation flux and anti-fouling property, but the hydrophilic PVP inclined to spillage during membrane separation progress. Subsequently, several publications reported that hydrophilic modification of membrane via blending with amphiphilic copolymers were successful since the permanent modification effect [18,19].

Recently, incorporating nano-materials such as SiO_2 [20–22], hydrous manganese dioxide [23], phosphorylated TiO_2-SiO_2 [24], and TiO_2 coated MWCNTs [25] with membrane matrix to prepare composite membrane has received widespread concerns due to the considerable improvement of the membrane properties such as hydrophilicity, permeability, mechanical strength and antifouling ability. Among the aforementioned nano-materials, SiO_2 NPs has became a prevalent material because of its easy preparation and outstanding chemical stability. However, if SiO_2 NPs without surface modification are directly blended with the hydrophobic membrane matrix, the miscibility is unsatisfactory due to the poor interfacial interaction between the hydrophobic membrane and hydrophilic SiO_2 [20–22]. Therefore, SiO_2 must be modified before incorporating into membrane matrix with the purpose to improve the compatibility between organic phase and inorganic phase. Yin and Zhou [7] used SiO_2-g-(PDMAEMA-co-PDMAPS) NPs as additive to fabricate PES composite membrane, which exhibited higher flux recovery and better anti-fouling property. Zhu et al. [26] first synthesized SiO_2-g-PHEMA NPs via surface-initiated RAFT polymerization, then the PES/SiO_2-g-PHEMA composite membrane with excellent anti-fouling property was fabricated.

In this work, highly hydrophilic SiO_2-g-PAA NPs are designed as modifier, has been synthesized by grafting hydrophilic PAA onto the SiO_2 NPs via surface-initiated ARGET ATRP. Then the PES/SiO_2-g-PAA composite membranes were fabricated by NIPS process. The effects of SiO_2-g-PAA NPs concentration on membranes performances, including porosity, permeation, hydrophilicity and antifouling ability of were comprehensive analyzed.

2. Experimental

2.1. Materials

PES (Mw = 150,000 g/mol) was purchased from Jida High Performance Materials Co., Ltd. Trifluoroacetic acid (TFA, 99%), N,N,N′,N′′,N′′-pentamethyldiethylenetriamine (PMDETA, 99%), copper (II) bromide ($CuBr_2$, 99.99%), sodium dodecyl sulfate (SDS, 99%), L-ascorbic acid (AA, 99%), 2-bromo-2-methylpropionylbromide (BiBB, 98%), 3-aminopropyltriethoxysilane (APTES, 99%), and N,N-dimethylacetamide (DMAc) were provided by Aladdin and used without purification. t-Butyl acrylate (t-BA, 98%) was supplied by Aldrich and passed through column chromatography of basic alumina oxide to remove the inhibitor. The toluene, tetrahydrofuran (THF) and dichloromethane used in this work were purified by distillation from CaH_2. The remaining chemical reagents were commercially analytical grade, and obtained from local chemical suppliers.

2.2. Synthesis of SiO_2-g-PAA NPs

The synthetic routes of SiO_2-g-PAA NPs are presented in Fig. 1 and described in the following steps.

2.2.1. Synthesis of 3-(2-bromoisobutyramido) propyl(triethoxy)-silane (APTES-BIBB)

The initiator, 3-(2-bromoisobutyramido)propyl (triethoxy)-silane, denoted as APTES-BIBB was synthesized as reported [7]. Yield 86%. ^{1}H NMR (300 MHz, $CDCl_3$, δ): 6.89 (s, 1H, –NH–CO–), 3.79–3.86 (q, 6H, $(CH_3–CH_2–O)_3Si–$), 3.24–3.30 (m, 2H, $–CH_2–NHCO–$), 1.95 (s, 6H, $–C(CH_3)_2–Br$), 1.61–1.73(m, 2H, $–CH_2–CH_2–NH–$), 1.21–1.26 (t, 9H, $(CH_3–CH_2–O)_3Si–$), 0.62–0.68 (t, 2H, $Si–CH_2–CH_2–$).

2.2.2. Synthesis of SiO_2-Br NPs

Monodispersed SiO_2 NPs were easily synthesized via Stöber sol-gel process [26]. In this work, the average size of the as-synthesized SiO_2 NPs was about 73 nm. Then, the initiator-immobilized SiO_2 NPs (SiO_2-Br) were synthesized via the condensation reaction of the triethoxysilane groups in APTES-BIBB with hydroxyl groups of SiO_2 NPs. Namely, 2 g of SiO_2 were dispersed into 200 mL toluene and sonicated for 2 h to produce a homogeneous suspension, 1.6 g of APTES-BIBB was added. Then the mixture was refluxed under nitrogen atmosphere for 12 h. After cooled to room temperature, the SiO_2-Br NPs were collected by centrifugation and washed with abundant toluene, dichloromethane and methanol to remove excess APTES-BIBB. Finally, the SiO_2-Br NPs were dispersed in methanol for subsequent polymerization.

2.2.3. Synthesis of SiO_2-g-PAA NPs

In this work, PAA coated SiO_2 NPs were synthesized via surface-initiated ARGET ATRP of t-butyl acrylate (tBA), followed by acid-catalyzed hydrolysis of t-butyl groups. Typically, in a round-bottomed flask, the SiO_2-Br NPs were dispersed in methanol and sonicated for 0.5 h to produce a homogeneous suspension. The resulting suspension was degassed by bubbling with nitrogen for 0.5 h. Degassed methanol solution containing PMDETA, tBA and $CuBr_2$ were then quickly added. The mixture was degassed by bubbling with nitrogen for 0.5 h. Finally, AA was introduced to activate polymerization (the molar ratio of tBA/

$CuBr_2$/PMDETA/AA was set as 4,000:1:10:10). The reaction was conducted at 50°C for 12 h with fierce stirring. After the polymerization, the SiO_2-g-PtBA NPs were collected by centrifugation, and washed with abundant dichloromethane and methanol. At last, the SiO_2-g-PtBA NPs were dispersed into methanol for subsequent acid-catalyzed hydrolysis reaction. Briefly, 5 mL TFA was added into aforementioned dispersion solution to conduct the hydrolysis reaction. After 24 h, the SiO_2-g-PAA NPs were collected, and washed with THF and methanol. At last, the SiO_2-g-PAA NPs were dispersed in DMAc for subsequent membrane fabrication.

2.3. Organic–inorganic composite membrane preparation [27]

The composite membranes were fabricated via the NIPS process. First, SiO_2-g-PAA NPs were dispersed into DMAc, after sonication for 0.5 h, PES was added to the solution. Then, the mixture was mechanically stirred for 24 h to obtain a homogeneous casting suspension. After removed bubbles, the casting solution was cast on a clean glass plate with 250 μm gap, exposed to air for 30 s and immediately immersed into a coagulation bath (deionized water) at 25°C. After the membrane was detached from the glass plate, the resultant membrane was thoroughly washed with deionized water before ultrafiltration. All of the membranes were fabricated under environmental humidity of 60% and temperature of 25°C. The fabricated PES/SiO_2-g-PAA membranes were named as PES/Si-A0.5, PES/Si-A1 and PES/Si-A2 according to the weight percentage of SiO_2-g-PAA NPs relative to the weight of casting solution. Similarly, the PES/SiO_2 composite membranes were also prepared, named as PES/Si0.5, PES/Si1 and PES/Si2, respectively. The PES blank membrane without NPs was fabricated named as PES. The compositions of the casting solution are shown in Table 1.

2.4. Characterization of SiO_2-g-PAA NPs and the fabricated membranes

^{1}H NMR spectra of the APTES-BIBB was recorded on an INOVA 300 MHz nuclear magnetic resonance instrument using $CDCl_3$. The surface chemical composition of NPs was surveyed by the Fourier transform infrared spectrometer (FITR, Bruker Tensor 27). Thermo gravimetric analysis (TGA, TA Q-600) was performed from 50°C to 800°C under N_2 atmosphere. The morphologies and particle sizes of SiO_2 NPs and SiO_2-g-PAA NPs were characterized by transmission electron microscopy (TEM, Hitachi H-600). The top surface and cross-sectional morphologies of the fabricated membranes were analyzed by SEM (Nova Nano SEM 430, FEI, USA).

The water contact angle instrument (JC-2000C1) was uesed to estimate the surface hydrophilicity of the fabricated membranes. Deionized water was dropped randomly on the surface of the tested membrane sample at five locations, and the average value was obtained. The membrane porosity (ε, %) was measured according to Eq. (1) [7,24]:

$$\varepsilon = \frac{\left(m_w - m_d\right)}{AL\rho} \times 100\% \tag{1}$$

where m_w (g), m_d (g), A (cm^2), L (cm) and ρ (g/cm^3) were the wet membrane weight, the dry membrane weight, the wet membrane effective area, the wet membrane thickness, and the pure water density, respectively. All measurements were repeated at least three times to minimize experimental error and the average values were acquired.

The Guerout–Elford–Ferry equation based on the flux and porosity data was used to calculate the mean pore size (r_m, nm) of membrane surface according to Eq. (2) [7,24]:

$$r_m = \sqrt{\frac{\left(2.9 - 1.75\varepsilon\right)8\eta l Q}{\varepsilon A \Delta P}} \tag{2}$$

where η (8.9 × 10^{-4} Pa s), Q (m^3/s), l (m), and ΔP (0.1 MPa) were the pure water viscosity, the volume of permeated pure water per unit time, the wet membrane thickness, and the operational pressure, respectively.

2.5. Permeability and antifouling performance of the fabricated membranes

The permeability and antifouling performance of the fabricated membranes were tested in accordance with the reported procedure [7]. The ultrafiltration was performed with a dead-end stirred cell filtration system (CB-380, 45.3 cm^2) at 25°C ± 1°C under a stirring speed of 400 rpm. Generally, four steps were included in one complete cycle. First, each membrane was initially pressurized at 1.6 bar with pure water until a steady flux was reached. After that, the pure water flux (PWF) was measured as J_{w1} at the 1.0 bar operation pressure. Next, oil-in-water emulsion (0.9 g/L, SDS as emulsifier) was used as the feed solution to permeating

Table 1
The compositions of the casting solution

Membranes	PES (wt.%)	Nanoparticle (wt.%)	DMAc (wt.%)
PES	15.0	0.0	85.0
PES/Si0.5	15.0	0.5 SiO_2	84.5
PES/Si1	15.0	1.0 SiO_2	84.0
PES/Si2	15.0	2.0 SiO_2	83.0
PES/Si-A0.5	15.0	0.5 SiO_2-g-PAA	84.5
PES/Si-A1	15.0	1.0 SiO_2-g-PAA	84.0
PES/Si-A2	15.0	2.0 SiO_2-g-PAA	83.0

through the membrane and stable oil water flux was acquired as J_{oil}. After 1 h of filtration, the fouled membrane was thoroughly rinsed with deionized water. Finally, the stable PWF of cleaned membrane was obtained as J_{w2}. The steady J_{w1}, J_{oil}, J_{w2} (L/m^2 h) were calculated according to Eq. (3):

$$J = \frac{V}{At} \tag{3}$$

where V (L), t (h), A (m^2) were the volume of permeated water, the filtration time, and the effective membrane area, respectively. The oil rejection (r) was calculated by Eq. (4):

$$r = \left(1 - \frac{C_p}{C_f}\right) \times 100\% \tag{4}$$

where C_p and C_f were the oil concentration of permeate and feed solutions, which were tested by UV-spectrophotometer (UV-9200).

The flux recovery ratios (FRR) was calculated using Eq. (5):

$$\text{FRR} = \frac{J_{w2}}{J_{w1}} \times 100\% \tag{5}$$

To evaluate the antifouling ability of membranes in detail, the flux loss caused by reversible fouling (R_r), irreversible fouling (R_{ir}) and total fouling (R_t) can be calculated as follows [7,24]:

$$R_r = \left(\frac{J_{w2} - J_{oil}}{J_{w1}}\right) \times 100\% \tag{6}$$

$$R_{ir} = \left(\frac{J_{w1} - J_{w2}}{J_{w1}}\right) \times 100\% \tag{7}$$

$$R_t = R_r + R_{ir} = \left(\frac{J_{w1} - J_{oil}}{J_{w1}}\right) \times 100\% \tag{8}$$

3. Results and discussions

3.1. Characterization of the SiO_2-g-PAA NPs

Fig. 1 depicts the preparation route of SiO_2-g-PAA NPs. To conduct surface-initiated ARGET ATRP from SiO_2 NPs, APTES-BIBB, a molecule containing an ARGET ATRP initiating site was beforehand synthesized via amidation reaction between APTES and BIBB, followed by silanization of triethoxysilane of APTES-BIBB on SiO_2 NPs surface, the SiO_2 NPs used in this study were synthesized by classical Stöber sol–gel process and the average diameter was about 73 nm (as shown in Fig. 6a). At last, the SiO_2-g-PAA NPs were synthesized via surface-initiated ARGET ATRP of tBA, followed by acid-catalyzed hydrolysis of t-butyl groups.

The structure of the APTES-BIBB was confirmed by ^{1}H NMR spectroscopy (as shown in Fig. 2). The integral ratio of signals at 6.89, 1.95 and 1.23 ppm were determined to be 1:6:9, indicating a quantitative transformation.

Fig. 3 represents the Fourier-transform infrared spectroscopy (FTIR) spectra of SiO_2, SiO_2-Br, SiO_2-g-PtBA and SiO_2-g-PAA NPs. Compared with the unmodified SiO_2 NPs, SiO_2-Br NPs exhibited two new absorption peaks at 2,918 and 2,860 cm^{-1}, which was attributed to C–H stretching of the CH_x (CH_3 and CH_2) groups in the APTES-BIBB, implying the initiator has been successfully immobilized

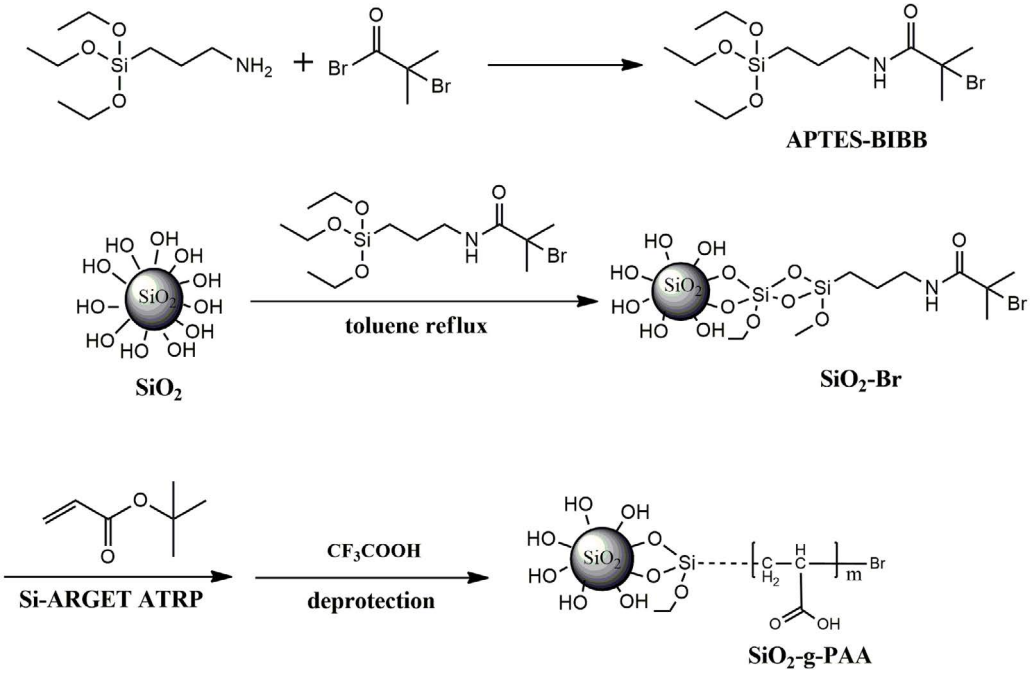

Fig. 1. Reaction procedure for preparation of SiO_2-g-PAA NPs.

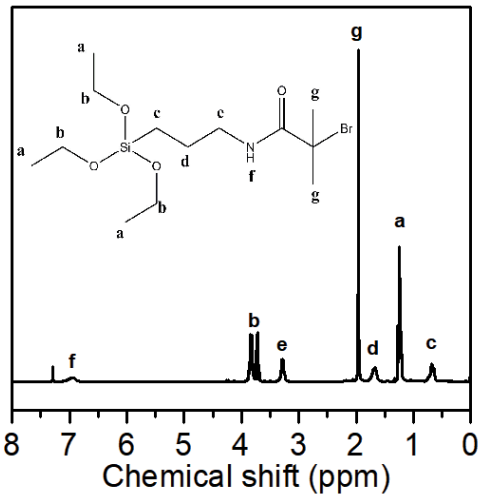

Fig. 2. ^{1}H-NMR spectra of APTES-BIBB in $CDCl_3$.

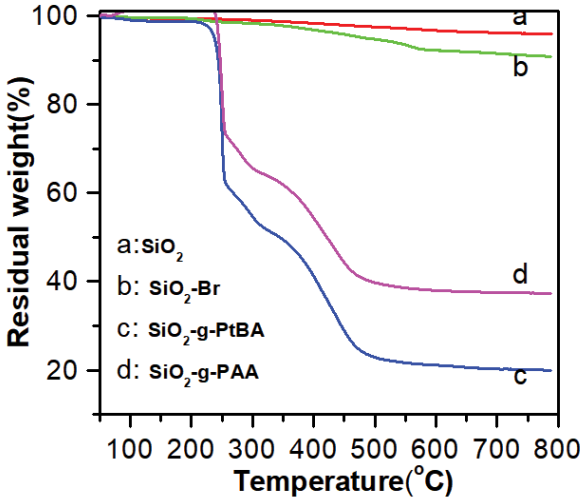

Fig. 4. TGA curves of (a) SiO_2, (b) SiO_2-Br, (c) SiO_2-g-PtBA, and (d) SiO_2-g-PAA.

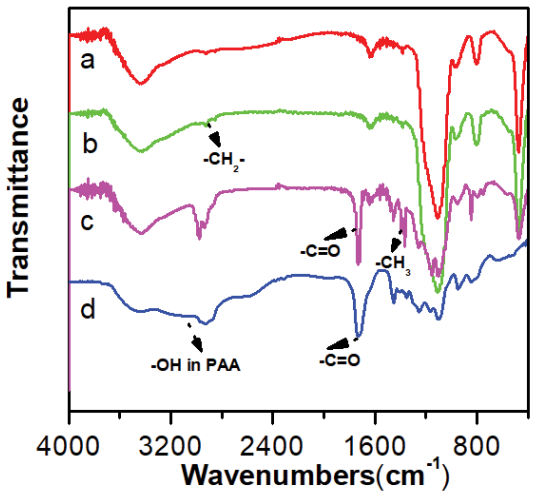

Fig. 3. FTIR spectra of (a) SiO_2, (b) SiO_2-Br, (c) SiO_2-g-PtBA, and (d) SiO_2-g-PAA.

onto the surface of SiO_2 NPs. In Fig. 3c the peak ascribed to C–H stretching of CH_x groups significantly enhanced. Additionally, absorption peaks at 1,730 and 1,380 cm^{-1} appeared, which are attributed to the C=O stretching vibration and bending vibration of CH_3 in the tert-butyl groups [28]. Compared with SiO_2-g-PtBA NPs, the absorption peak at 1,380 cm^{-1}, representing the CH_3 in tert-butyl side chains almost complete disappeared after treatment with TFA, and the broad absorption peak between 3,300 and 2,700 cm^{-1} was appeared, which ascribed to the hydroxyl group in –COOH [28]. Furthermore, the C=O stretching vibration peak shifted from 1,730 to 1,710 cm^{-1}, indicating the successful grafted the PAA chains onto the SiO_2 NPs surface.

In order to further verified the surface modification of SiO_2 NPs, TGA curves of SiO_2, SiO_2-Br, SiO_2-g-PtBA and SiO_2-g-PAA NPs are depicted in Fig. 4. The weight losses of SiO_2, SiO_2-Br, SiO_2-g-PtBA, and SiO_2-g-PAA NPs were 4.13%, 9.18%, 80.03% and 62.68%, respectively. After the hydrolysis of SiO_2-g-PtBA NPs with the trifluoroacetic acid, percent of organic components in the case of SiO_2-g-PAA NPs significantly dropped due to the removal of t-BA groups (Fig. 4d).

TEM images of the bare unmodified SiO_2 and SiO_2-g-PAA NPs are depicted in Fig. 5. Clearly, the SiO_2 NPs aggregated seriously and difficult to distinguished one particle from the other. After the introduction of PAA shell, the dispersibility of the SiO_2-g-PAA NPs improved remarkably (Fig. 5b). Furthermore, the high magnification TEM images of individual SiO_2-g-PAA NPs illustrated that a stable and dense polymer shell was directly coated on the surface of the SiO_2 NPs (Fig. 5d) and the diameter of the NPs was around 77 nm, which was larger than unmodified SiO_2 NPs (73 nm). Combined with the analysis of FTIR, TGA and TEM, it was reasonable to assume that the core-shell structured SiO_2-g-PAA NPs had been successfully synthesized.

3.2. Surface enrichment behavior of SiO_2-g-PAA NPs during membrane formation process

To investigate surface chemical structures of the synthesized membranes, ATR-FTIR spectra are provided in Fig. 6. Cleanly, the PES/Si-A1 composite membrane presented very similar spectra compared with the PES blank membrane, except the distinct peak at about 1,720 cm^{-1}, which was attributed to the stretching vibration of carboxyl group in PAA chain of SiO_2-g-PAA NPs, indicating the existence of SiO_2-g-PAA NPs in the near surface of the composite membrane. The surface enrichment of SiO_2-g-PAA NPs during membrane formation process is schemed in Fig. 7. In membrane formation process, PES coagulated promptly to form the membrane matrix and the hydrophilic SiO_2-g-PAA NPs migrated spontaneously to the membrane surface to reduce interfacial energy, the similar phenomenon was reported in other literature [7,26]. In addition, the surface enrichment behavior of SiO_2-g-PAA NPs was

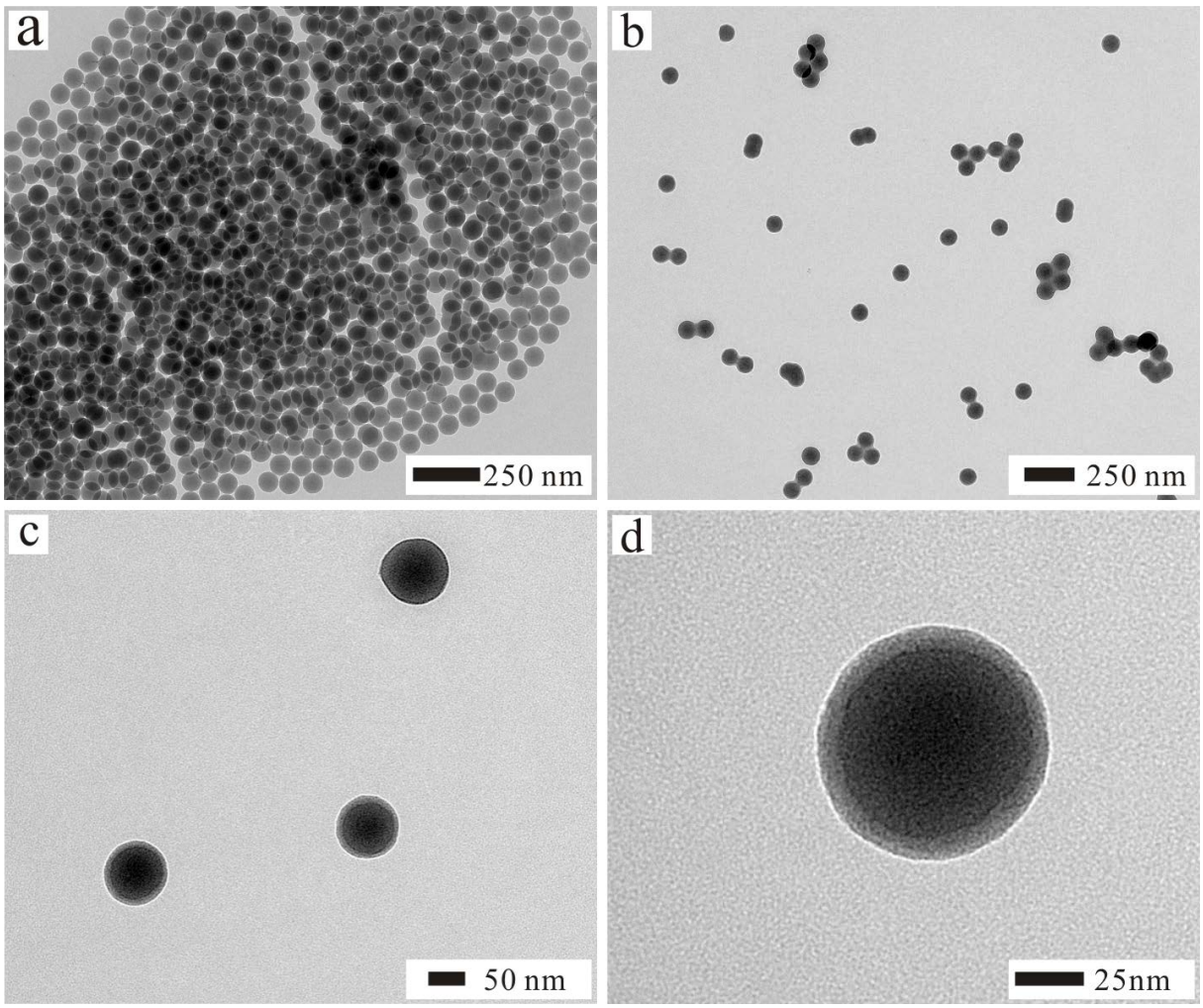

Fig. 5. TEM images of NPs dispersed in DMAc: SiO_2 (a) and SiO_2-g-PAA (b–d).

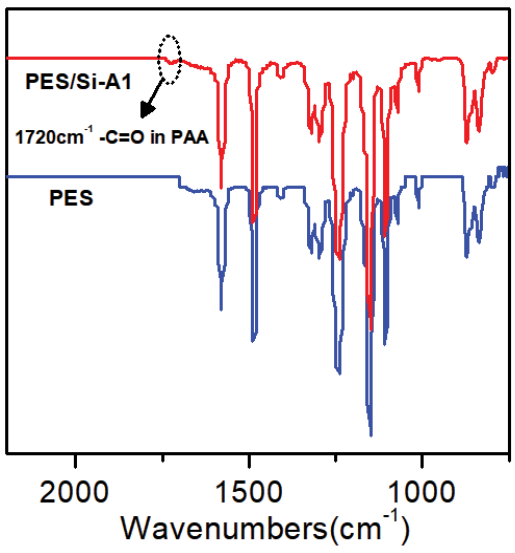

Fig. 6. ATR-FTIR spectra of PES membrane and PES/Si-A1 membrane.

also confirmed by SEM (as shown in Fig. 8f), which was discussed in the section 3.3 in detail.

3.3. Morphologies of membranes

The surface and cross-section morphologies of PES blank membrane, PES/Si1 and PES/Si-A1 composite membranes were observed. As shown in Fig. 8, there was no appreciable cross-sectional morphological variation between the unmodified PES blank membrane and the modified composite membrane, all tested membranes exhibited asymmetric structures, including a wafery dense top-layer, a porous finger-like sub-layer and fully developed macrovoid, which were similar to our early report [7]. The composite membranes had higher porosity and larger surface pore size than PES blank membrane (Fig. 9). Clearly, the unmodified PES membrane had conspicuous macrovoids structure in the sublayer. It is generally recognized that the macrovoids structure were regularly existed in the membrane which had a dense skin layer [29]. The unmodified PES membrane had the smallest surface pore size, which hindered water diffusing into the sublayer and resulted in the formation of the macrovoids structure [7,29]. Compared with PES membrane, the

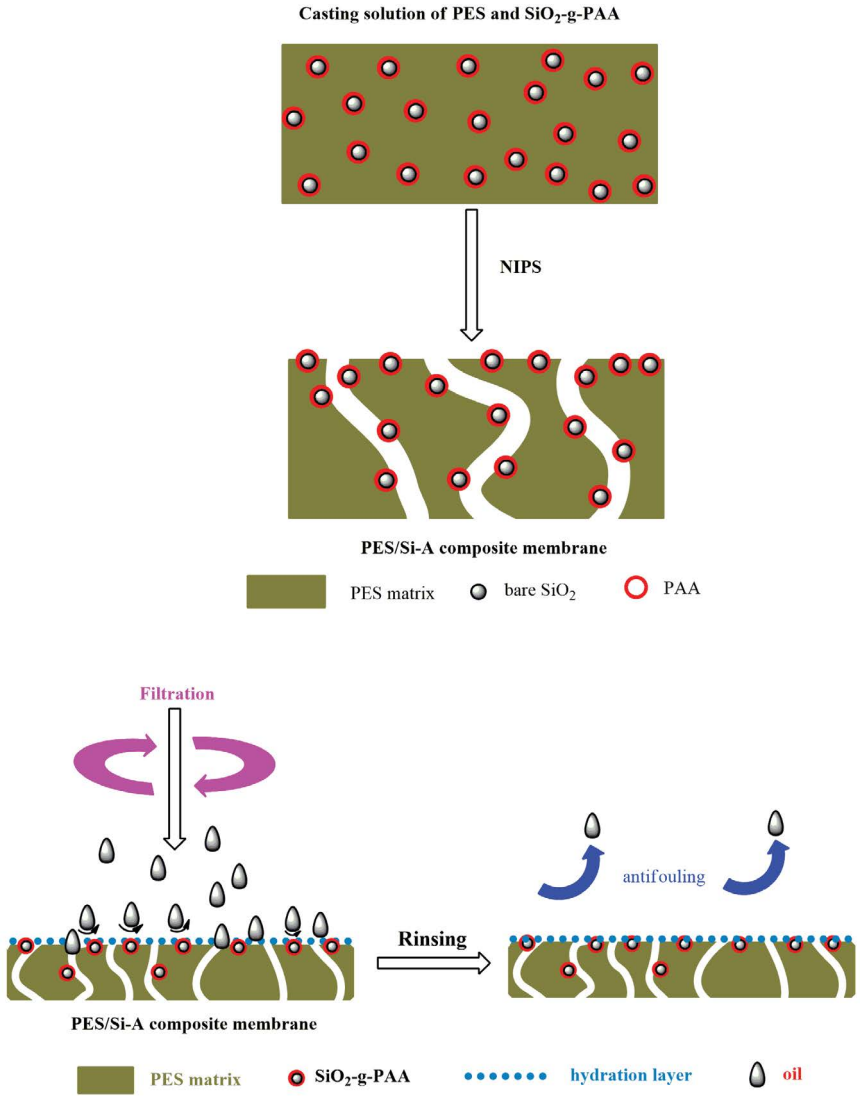

Fig. 7. Schematic illustration for the surface enrichment behavior of SiO_2-g-PAA NPs during membrane formation and antifouling performance of the PES/Si-A composite membrane.

cross-section morphologies of PES/Si-A1 composite membranes exhibited that macrovoids structure were suppressed and the finger-like pores became longer. Since the PES/Si-A1 composite membrane had larger surface pore size compare to the PES membrane, water molecules could diffuse easier into the sublayer, which induced many nuclei formation and suppressed the formation of macrovoids structure [7,29]. Clearly, as shown in Fig. 8d, the PES/Si1 membrane surface contained a small amount of agglomerated SiO_2 NPs. By contrast, the well-dispersed SiO_2-g-PAA NPs were easier to migrate onto the membrane surface and distributed evenly, agglomerated NPs almost unobservable (Fig. 8f).

3.4. Porosity, mean pore size, hydrophilicity and mechanical properties of the composite membranes

The porosity and mean pore size of the PES blank membrane, PES/Si and PES/Si-A composite membranes were quantitatively calculated and depicted in Fig. 9. Obviously, the porosity and mean pore size of the composite membranes (PES/Si and PES/Si-A) were remarkably higher than PES blank membrane. Moreover, with increasing concentration of SiO_2 NPs and SiO_2-g-PAA NPs, the composite membranes porosity and mean pore size increased initially, reached to the maximum when the NPs concentration was 1.0 wt.%. After that, they decreased with the further increasing of NPs concentration. The variation trend was similar to other studies [30] and could be interpreted as follows. Firstly, the introduction of NPs to the casting solution enhanced the thermodynamic instability of the system, which promoted phase separation happen at a low polymer concentration [24], resulting in the formation of large surface pore size and high surface porosity. Secondly, during the NIPS process, the hydrophilic NPs spontaneously migrated to the membrane top surfaces in order to minimization the interfacial energy between membrane and coagulation bath [7,26].

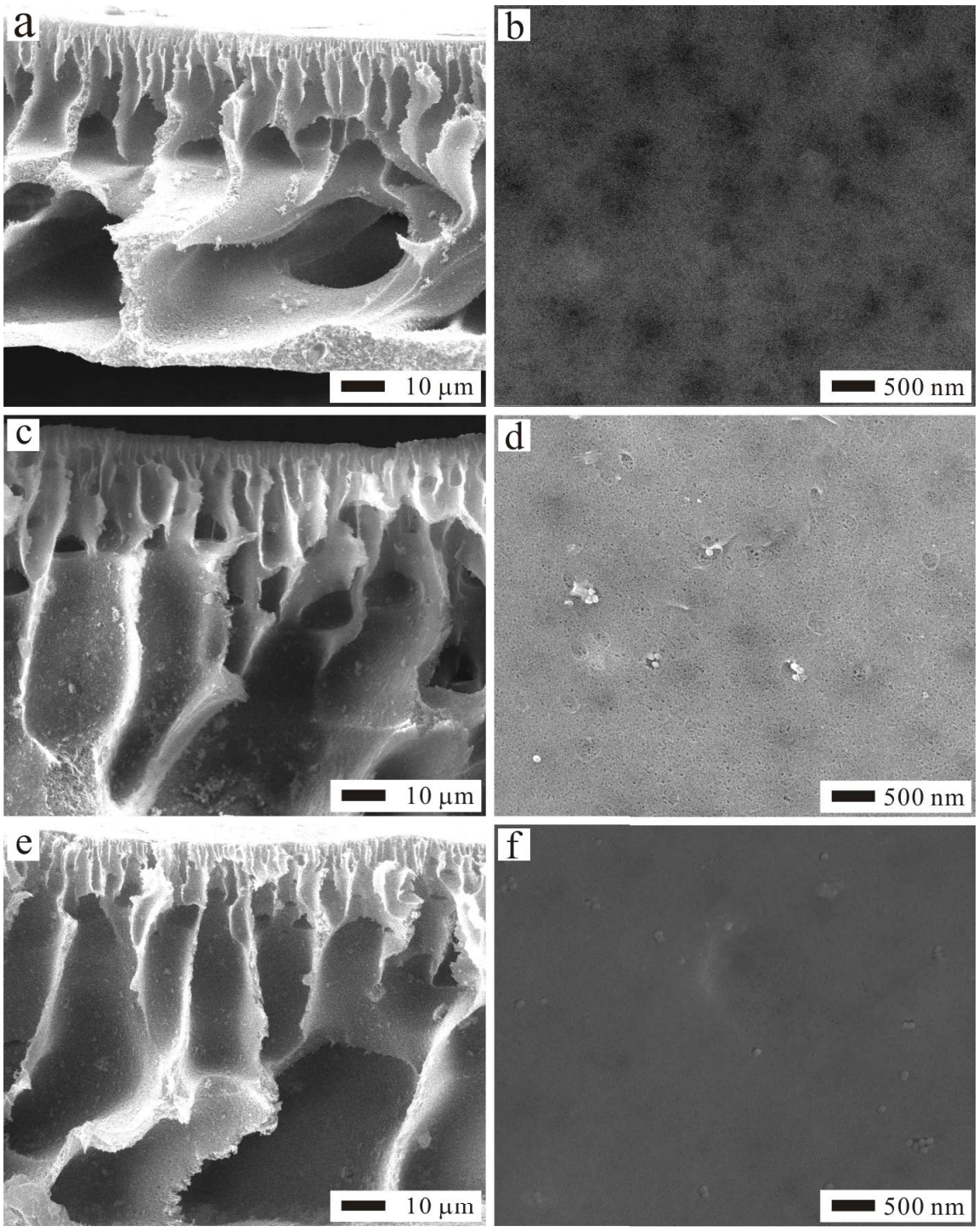

Fig. 8. Surface morphologies of the tested membranes: (b) PES, (d) PES/Si1, (f) PES/Si-A1; Cross-sectional morphologies of the tested membranes: (a) PES, (c) PES/Si1, (e) PES/Si-A1.

Meanwhile, a little of NPs acted as pore-forming agent leached out from membrane matrix, resulting in the membrane have high porosity and large surface pore size [7]. Lastly, with increasing the NPs concentration, the viscosity of the casting solution system notably increased, which resulted in a delayed demixing. As a result, the membrane with low porosity and small mean pore size would formation. Compared to the PES/Si composite membranes, the PES/Si-A membranes had higher porosity and larger surface pore size.

The membrane surface hydrophilicity has crucial effect on permeation and antifouling property of membranes. In present study, the static water contact angle was measured to evaluate the membrane hydrophilicity and the results

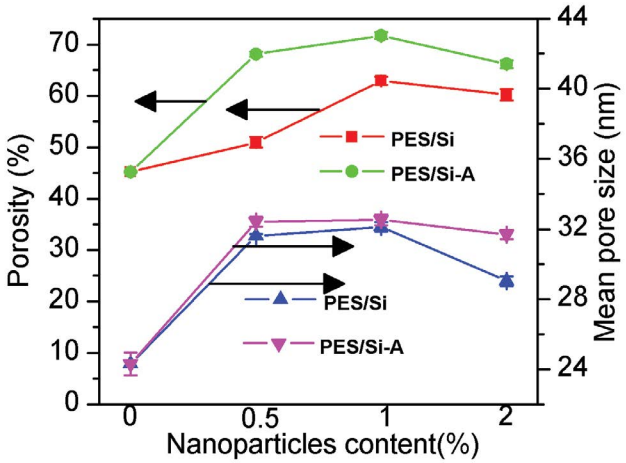

Fig. 9. Effect of NPs concentration on porosity and mean pore size of PES/Si and PES/Si-A composite membranes. Data were means ± SD (n = 3).

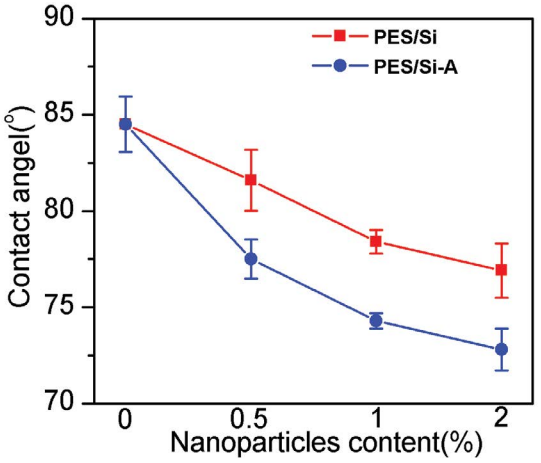

Fig. 10. Effect of NPs concentration on static water contact angle of PES/Si and PES/Si-A composite membranes. Data were means ± SD (n = 3).

are depicted in Fig. 10. The lower contact angle indicates the higher hydrophilic property of the membrane. Clearly, the PES blank membrane had the highest water contact angle around 84.5°, representing poor hydrophilicity. With increasing the NPs concentration, the contact angles of the membranes decreased gradually. As for the PES/Si composite membranes, the contact angle slightly decreased relative to the PES blank membrane, implying that the addition of unmodified SiO_2 NPs restricted improvement hydrophilicity. Comparatively, the PES/Si-A composite membranes exhibited better hydrophilicity, the contact angle decreased to 72.8° when the concentration of SiO_2-g-PAA NPs was 2.0 wt.%. It can be interpreted by three aspects. Firstly, SiO_2-g-PAA NPs had considerable hydrophilic PAA groups, resulting in the PES/Si-A membranes surface more hydrophilic than the PES/Si membranes. Secondly, the serious aggregation of the unmodified SiO_2 NPs, which significantly reduced the effective surface of the NPs, resulting in the decrease of the hydrophilic hydroxyl groups on the surface of PES/Si membranes [31]. Lastly, compared to the unmodified SiO_2, the well-dispersed SiO_2-g-PAA NPs were easier to migrate onto the membrane surface, endowing the PES/Si-A composite membranes better hydrophilicity. Furthermore, the surface free energy was frequently determined by the contact angles of probe liquids on the membrane surface. The total surface energy of the unmodified PES membrane was lowest, around 37.6 mJ/m^2. The total surface energies of the PES/Si and PES/Si-A composite membranes were increased after addition the NPs (SiO_2 and SiO_2-g-PAA), because of the spontaneous surface segregation of the hydrophlic NPs onto the surface (Figs. 6 and 8), and finally reached a max value of 46.9 mJ/m^2 (PES/Si-A2 membrane).

The mechanical strength of unmodified PES membrane and modified composite membranes are listed in Table 2. As shown in Table 2, the mechanical strength of composite membranes increased firstly and then decreased and all higher than that of PES membrane. Among the fabricated composite membranes, the mechanical strength of PES/Si-A membrane were superior to those of PES/Si membrane. Compared to the unmodified SiO_2 NPs, SiO_2-g-PAA NPs were more likely to form hydrogen bonds with PES due to carboxylic groups on the surface (–COOH with S=O), which might make the PES molecular chains tighter and improve mechanical property of the composite membranes.

3.5. Separation and antifouling performance of the composite membranes

The effect of SiO_2 NPs and SiO_2-g-PAA NPs concentration on PWF, oil flux, oil rejection of PES/Si and PES/Si-A composite membranes are shown in Fig. 11. Obviously, the oil rejection of the PES blank membrane and composite membranes were 100%, indicating excellent oil removal efficiency. As depicted in Fig. 11a, the PES blank membrane had the lowest PWF around 64.10 L/m^{2}h. After introduction of the NPs, the PWF was dramatically changed, it increased at first and reached to the maximum when the NPs concentration was 1.0 wt.%. Subsequently, the value decreased with higher NPs concentration (2.0 wt.%) in the casting solution. Similar results were reported in previous

Table 2
Tensile strength of unmodified PES and modified composite membranes

	PES	PES/Si0.5	PES/Si1	PES/Si2	PES/Si-A0.5	PES/Si-A1	PES/Si-A2
Tensile strength (MPa)	2.21	2.65	2.87	2.73	2.79	3.12	2.97

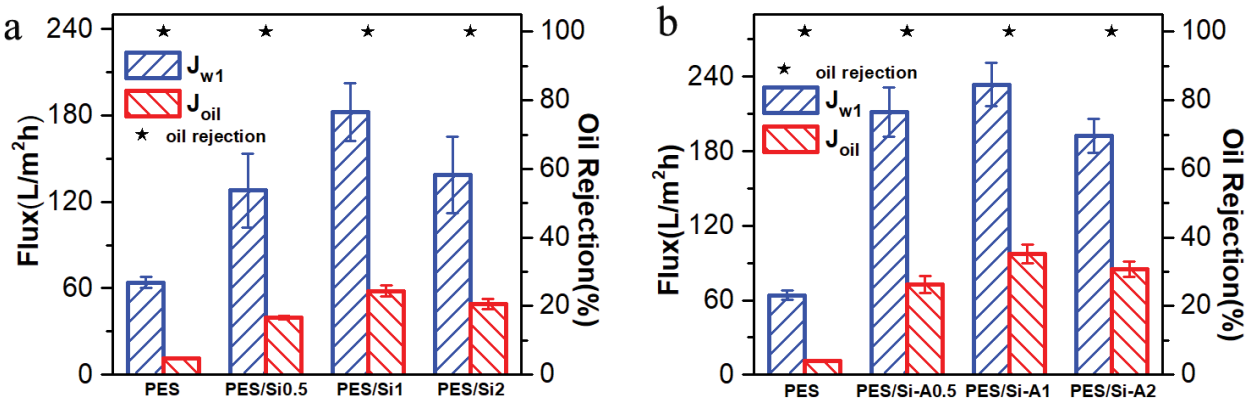

Fig. 11. Effect of NPs concentration on J_{w1}, J_{oil}, and oil rejection of the PES/Si (a) and PES/Si-A membranes (b), data were means ± SD (n = 3).

literature [7]. The change of oil water flux maintained the same trend with PWF. It is widely accepted that the permeation flux is determined by the porosity, mean pore size and hydrophilicity of the membrane [7,26]. The synergetic effect of porosity and hydrophilicity should be considered. When NPs concentration was 1.0 wt.%, the PES/Si1 and PES/Si-A1 membranes had highest porosity (as shown in Fig. 9) and medium hydrophilicity (as shown in Fig. 10), which exhibited the highest pure water flux and oil water flux (182.37 and 58.22 L/m² h for PES/Si1 membrane, 233.72 and 97.29 L/m² h for PES/Si-A1 membrane). When 2.0 wt.% NPs were added into the casting solution, the hydrophilicity of PES/Si2 and PES/Si-A2 membranes were higher than that of PES/Si1 and PES/Si-A1 membranes. Theoretically, the enhanced hydrophilicity can reduce effectively the resistance between water molecules and the membrane pores, which enhanced the permeation flux of membrane [32]. However, the PES/Si2 and PES/Si-A2 membranes had the decreased permeation flux, which might be result from the influence of the porosity was more significant.

Fig. 12 presents time-dependent fluxes of PES, PES/Si and PES/Si-A membranes of the complete ultrafiltration experiment. In the initial stage (1 h pure water filtration), the J_{w1} of composite membranes (PES/Si, PES/Si-A) were higher than PES blank membrane because of the increased surface porosity and improved hydrophilicity. Then, the J_{oil} attenuated sharply at few minutes of filtration, which was attributed to the oil droplets blocked the membrane pores. Subsequently, the J_{oil} kept stable due to the adsorption and diffusion of oil droplets reached dynamic balance [5]. After washing the fouled membranes, the J_{w2} was obtained, then FRR was calculated according to Eq. (5) and the results are presented in Fig. 13. It can be seen that the FRR of PES/Si-A membranes (64.20%, 68.34%, 77.12% for the PES/Si-A0.5, PES/Si-A1, PES/Si-A2, respectively) were higher compared to the PES/Si membranes (57.99%, 61.19%, 73.23% for the PES/Si0.5, PES/Si1, PES/Si2, respectively) and PES blank membrane (45.75%). It is widely recognized that higher FRR mean lower tendency to be fouled. The results indicated that the antifouling performance of PES/Si-A

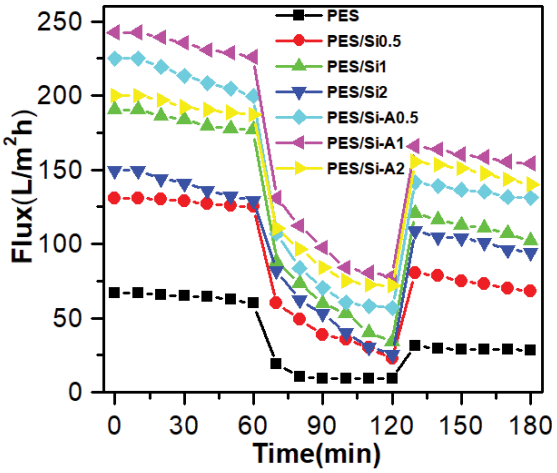

Fig. 12. Time-dependent fluxes of tested membranes during the complete ultrafiltration. The process includes four steps: pure water flux ultrafiltration (0–60 min), oil-in-water emulsions ultrafiltration (60–120 min), water washing (not shown), and pure water flux ultrafiltration of the cleaned membranes (120–180 min).

composite membranes was significantly enhanced compared to the PES blank membrane.

Furthermore, based on the fluxes (J_{w1}, J_{oil}, J_{w2}), R_r, R_{ir} and R_t were quantitatively calculated to analyze the membrane fouling in detail. The values of R_r, R_{ir} and R_t are presented in Fig. 14. Clearly, the PES blank membrane had highest R_t value, around 82.70%, indicating that the PES blank membrane underwent serious fouling. As for the PES/Si composite membranes, the R_t reduced to 69.15% (PES/Si0.5), 68.01% (PES/Si1), and 64.68% (PES/Si2), implying lower total flux loss. By contrast, the PES/Si-A membranes presented lower R_t and R_{ir}, which proved that membrane fouling caused by oil adsorption could be effectively restricted by incorporation of the hydrophilic SiO_2-g-PAA NPs on PES membrane surface. At the same time, the percentage of reversible fouling in total fouling (R_r/R_t) increased with

the increasing NPs concentration (as shown in Fig. 14c). Especially, when the concentration of SiO_2-g-PAA NPs was 2 wt.%, the R_r/R_t value reached 58.97%, which was notably higher than that of PES blank membrane (34.40%). Therefore, the flux of PES/Si-A composite membranes can be recovered effective just by simple water cleaning.

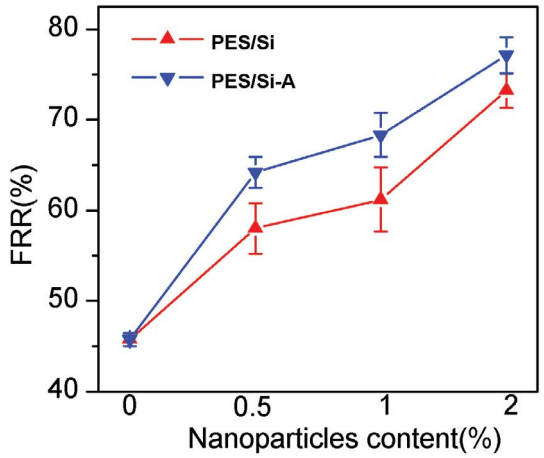

Fig. 13. Effect of NPs content on FRR of PES/Si and PES/Si-A membranes. Data were means ± SD (n = 3).

Furthermore, the PES membrane and modified PES/Si-A1 composite membrane were subjected to three cycles of complete filtration test. The initial PWF of the PES membrane was 64.10 L/m²h, and after three cycles of filtration, it decreased to 17.1 L/m²h. The initial PWF of the PES/Si-A1 composite membrane was around 233.72 L/m²h, and it was still as high as 175.8 L/m²h after three cycles of filtration, the flux recovery rates were 77.12%, 75.39%, and 75.21%, respectively, suggesting excellent stability.

Table 3 lists the pure water flux, oil/water flux and flux recovery rate of the PES/Si-A1 composite membrane prepared in this work and PES-based composite membrane reported in other literature. Compared with other PES base composite membranes, PES/Si-A1composite membrane had excellent permeation flux and anti-fouling performance, and provided theoretical guidance for the development of high-performance anti-fouling organic-inorganic composite membrane.

3.6. Stability of the SiO_2-g-PAA NPs in the composite membranes

The stability of NPs in the organic-inorganic composite membrane matrix is crucial in the practical application of oil-in-water emulsion ultrafiltration, if the NPs leak out from the membrane matrix, the membrane performances that including oil rejection, hydrophilicity and antifouling ability will decline inevitably. In this study, the

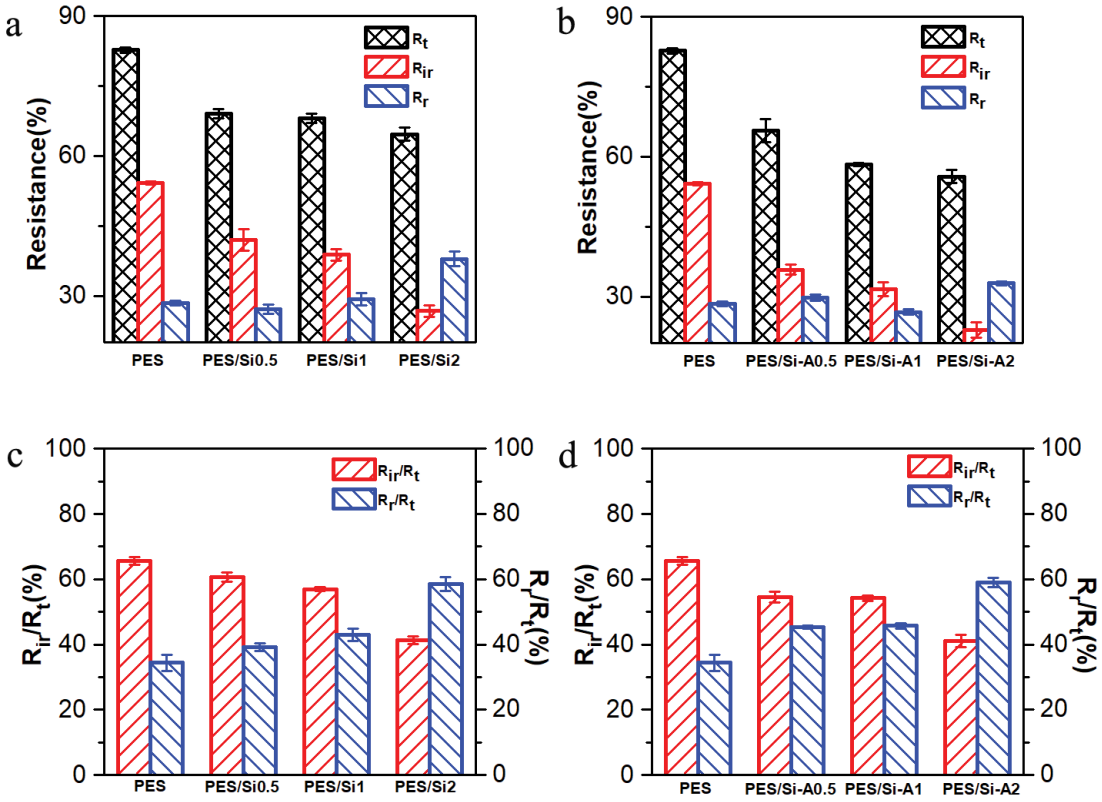

Fig. 14. Summary of the R_t, R_{ir} and R_r for (a) PES/Si and (b) PES/Si-A composite membrane. The ratio of R_r and R_{ir} to the R_t for (c) PES/Si and (d) PES/Si-A composite membrane. Data were means ± SD (n = 3).

Table 3
Comparison of PES/Si-A1 membrane with other PES membranes on pure water flux, oil–water flux and the flux recovery ratio

Membrane	Pure water flux (L/m^{2}h)	Oil/water flux (L/m^{2}h)	FRR (%)	References
PES/SiO_2-g-PHEMA	208.68	86.86	78.32	[34]
PES/SiO_2-g-(PDMAEMA-co-PDMAPS)	172.30	79.83	84.26	[7]
PES/Pluronic F127	130.20	82.98	63.40	[5]
F3-PDA/PES	40.20	46.10	93.40	[33]
PES/Si-A1	233.72	97.29	77.12	This work

PES/Si1 and PES/Si-A1 membranes were chosen, which were continuously shaken at 50°C for different time span (2, 4, 6, 8, 10 d). During the shaking, deionized water as the solvent was replaced every day. Then, the membranes were detected by water contact angle. In addition, surface SEM and ATR-FTIR of the membranes were also used to evaluate the stability of the NPs.

Fig. 15 presents the surface SEM images of the original PES/Si-A1 membrane and the membrane after washing for 10 d. As depicted in Fig. 15a, the SiO_2-g-PAA NPs distributed evenly on the surface of the membrane, after washing for 10 d, the number of the SiO_2-g-PAA NPs on the surface of the membrane almost unchanged, indicated the SiO_2-g-PAA NPs can stably entrap in the PES matrix. In addition, the ATR-FTIR presented in Fig. 16a was also employed to investigate the SiO_2-g-PAA NPs stability. As discussed in the section 3.3, the peak at about 1,720 cm^{-1} was attributed to the stretching vibration of carboxyl group in PAA chain of SiO_2-g-PAA NPs. Compared with the original PES/Si-A1 membrane, the intensity of the peak was almost unchanged, showing tiny SiO_2-g-PAA NPs leaked from the PES matrix. As presented in Fig. 16b, the test membranes surface contact angle gradually increased with the increasing of the shaking time. The contact angle of the original PES/Si1 membrane was about 78.4°, it increased 13.1% and reached to 88.7° after shaking for 10 d. As for PES/Si-A1 membrane, the contact angle after washing for 10 d (77.2°) was slightly higher than that of the original membrane (74.3°), it only increased 3.9%. It is reasonable that the poor interaction between the hydrophobic PES and the hydrophilic NPs make the NPs be liable to leach out from the membrane during shaking. Compared to the unmodified SiO_2 NPs, the PAA chains of SiO_2-g-PAA NPs entangled and interacted with PES strongly, which make the SiO_2-g-PAA NPs stably entrap in the composite membrane in the practical ultrafiltration.

4. Conclusions

In this work, the well dispersed SiO_2-g-PAA NPs were successfully prepared via Si-ARGET ATRP. Then, a convenient strategy for fabricating organic-inorganic composite membranes was established by the NIPS process. The porosity, mean pore size, pure water flux and oil flux of membrane increased initially by incorporation of low amount of SiO_2 NPs and SiO_2-g-PAA NPs. Then, they reached maximum when the NPs dosage was 1.0 wt.%, and decreased with continuous increasing of NPs concentration, which could be attributed to the synergetic effect between the thermodynamic enhancement and the rheological hindrance. In membrane formation process, the hydrophilic SiO_2-g-PAA NPs migrated spontaneously to the membrane surface to minimize interfacial energy. Thus, the hydrophilicity, permeability and antifouling property of PES/

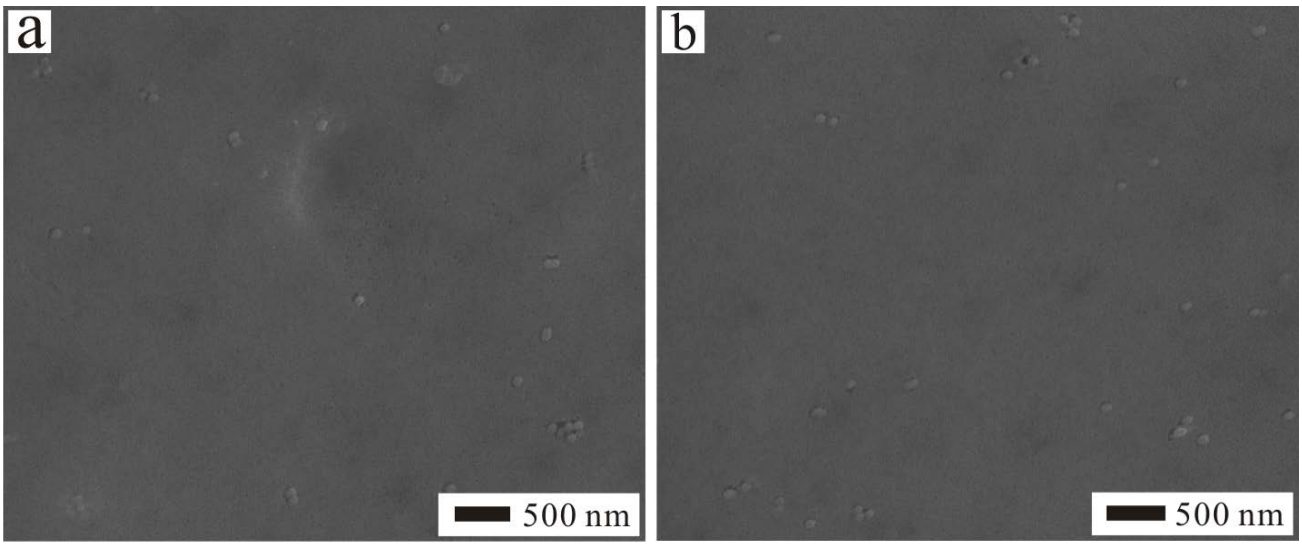

Fig. 15. SEM images of the original PES/Si-A1 (a) and washing for 10 d (b) in a pure water bath under shaking (100 rpm) at 50°C.

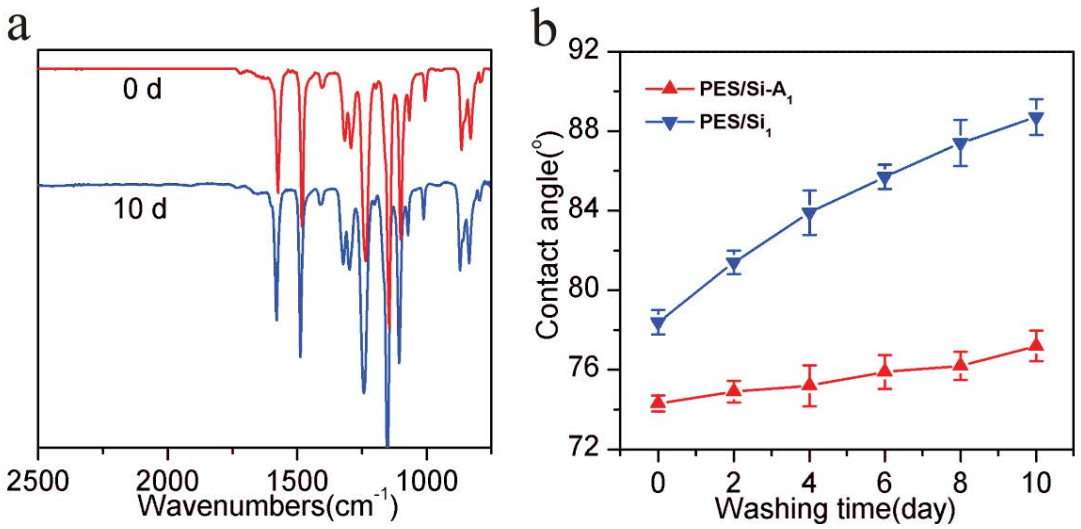

Fig. 16. (a) ATR-FTIR spectra of PES/Si-A1 membrane before and after shaken in water for 10 d and (b) water contact angles of PES/Si1 and PES/Si-A1 membranes after shaken in water for different days.

Si-A composite membrane were significantly improved. Moreover, the SiO_2-g-PAA NPs had better dispersibility in comparison with the unmodified SiO_2 NPs. At the same time, the interaction of PAA and PES improved the bonding ability between the SiO_2-g-PAA NPs and the PES membrane matrix, which made the NPs stably entrapped in the PES membrane, exhibiting excellent durability. More interestingly, the highly reactive PAA chains on the NPs provide a platform for further membrane surface functionalization, the next, we will grafting the amphiphilic block copolymer on the surface of the membrane to endow the antifouling and self-cleaning properties of composite membrane.

Acknowledgment

This work was supported by the Jiang xi Provincial Sci & Tech Plan of China (Grant No. GJJ202805) and Jing de Zhen Sci & Tech Plan of China (Grant No.2017GYZD021-03).

References

[1] S. Mondal, S. Ranil Wickramasinghe, Produced water treatment by nanofiltration and reverse osmosis membranes, J. Membr. Sci., 322 (2008) 162–170.
[2] M.A. Shannon, P.W. Bohn, M. Elimelech, J.G. Georgiadis, B.J. Marinas, A.M. Mayes, Science and technology for water purification in the coming decades, Nature, 452 (2008) 301–310.
[3] J. Kong, K. Li, Oil removal from oil-in-water emulsions using PVDF membranes, Sep. Purif. Technol., 16 (1999) 83–93.
[4] A. Mansourizadeh, A. Javadi Azad, Preparation of blend polyethersulfone/cellulose acetate/polyethylene glycol asymmetric membranes for oil–water separation, J. Polym. Res., 21 (2014) 1–9.
[5] W.J. Chen, J.M. Peng, Y.L. Su, L.L. Zheng, L.J. Wang, Z.Y. Jiang, Separation of oil/water emulsion using Pluronic F127 modified polyethersulfone ultrafiltration membranes, Sep. Purif. Technol., 66 (2009) 591–597.
[6] B. Chakrabarty, A. Ghoshal, M. Purkait, Ultrafiltration of stable oil-in-water emulsion by polysulfone membrane, J. Membr. Sci., 325 (2008) 427–437.
[7] J. Yin, J.C. Zhou, Novel polyethersulfone hybrid ultrafiltration membrane prepared with SiO_2-g-(PDMAEMA-co-PDMAPS) and its antifouling performances in oil-in-water emulsion application, Desalination, 365 (2015) 46–56.
[8] A. Rahimpour, S.S. Madaeni, Polyethersulfone (PES)/cellulose acetate phthalate (CAP) blend ultrafiltration membranes: preparation, morphology, performance and antifouling properties, J. Membr. Sci., 305 (2007) 299–312.
[9] Q.F. Alsalhy, Hollow fiber ultrafiltration membranes prepared from blends of poly (vinyl chloride) and polystyrene, Desalination, 294 (2012) 44–52.
[10] D. Kim, H. Kang, S Han, J.-C. Lee, The increase of antifouling properties of ultrafiltration membrane coated by star-shaped polymers, J. Mater. Chem., 22 (2012) 8654–8661.
[11] B.D. Mccloskey, H. Ju, B.D. Freeman, Composite membranes based on a selective chitosan-poly (ethylene glycol) hybrid layer: synthesis, characterization, and performance oil-in-water purification, Ind. Eng. Chem. Res., 49 (2009) 366–373.
[12] R. Revanur, B. Mccloskey, K. Breitenkamp, B.D. Freeman, T. Emrick, Reactive amphiphilic graft copolymer coatings applied to poly(vinylidene fluoride) ultrafiltration membranes, Macromolecules, 40 (2007) 3624–3630.
[13] H. Ju, B.D. Mccloskey, A.C. Sagle, Y.-H. Wu, V.A. Kusuma, B.D. Freeman, Crosslinked poly(ethylene oxide) fouling resistant coating materials for oil/water separation, J. Membr. Sci., 307 (2008) 260–267.
[14] D. Wandera, S.R. Wickramasinghe, S.M. Husson, Modification and characterization of ultrafiltration membranes for treatment of produced water, J. Membr. Sci., 373 (2011) 178–188.
[15] M.A. Masuelli, M. Grasselli, J. Marchese, N. Ochoa, Preparation, structural and functional characterization of modified porous PVDF membranes by γ-irradiation, J. Membr. Sci., 389 (2012) 91–98.
[16] W.J. Chen, Y.L. Su, L.L. Zheng, L.J. Wang, Z.Y. Jiang, The improved oil/water separation performance of cellulose acetate-graft-polyacrylonitrile membranes, J. Membr. Sci., 337 (2009) 98–105.
[17] J. Marchese, M. Ponce, N.A. Ochoa, P. Prádanos, L. Palacio, A. Hernández, Fouling behaviour of polyethersulfone UF membranes made with different PVP, J. Membr. Sci., 211 (2003) 1–11.
[18] T. Rajasekhar, M. Trinadh, P.V. Babu, A.V. Sesha, S.A.V.R. Reddy, Oil-water emulsion separation using ultrafiltration membranes based on novel blends of poly(vinylidene fluoride) and amphiphilic tri-block copolymer containing carboxylic acid functional group, J. Membr. Sci., 481 (2015) 82–93.
[19] X. Zhao, W. Chen, Y. Su, W. Zhu, J. Peng, Z. Jiang, L. Kong, Y. Li, J. Liu, Hierarchically engineered membrane surfaces with

superior antifouling and self-cleaning properties, J. Membr. Sci., 441 (2013) 93–101.
[20] A. Ahmad, M. Majid, B. Ooi, Functionalized PSf/SiO_2 nanocomposite membrane for oil-in-water emulsion separation, Desalination, 268 (2011) 266–269.
[21] M.S. Muhamad, M.R. Salim, W.J. Lau, Preparation and characterization of PES/SiO_2 composite ultrafiltration membrane for advanced water treatment, Korean J. Chem. Eng., 32 (2015) 2319–2329.
[22] J.N. Shen, H.M. Ruan, L.G. Wu, C.J. Gao, Preparation and characterization of PES-SiO_2 organic-inorganic composite ultrafiltration membrane for raw water pretreatment, Chem. Eng. J., 168 (2011) 1272–1278.
[23] R.J. Gohari, E. Halakoo, W. Lau, M. Kassim, T. Matsuura, A. Ismail, Novel polyethersulfone (PES)/hydrous manganese dioxide (HMO) mixed matrix membranes with improved antifouling properties for oily wastewater treatment process, RSC Adv., 4 (2014) 17587–17596.
[24] Y. Zhang, F. Liu, Y. Lu, L. Zhao, L. Song, Investigation of phosphorylated TiO_2-SiO_2 particles/polysulfone composite membrane for wastewater treatment, Desalination, 324 (2013) 118–126.
[25] V. Vatanpour, S.S. Madaeni, R. Moradian, S. Zinadini, B. Astinchap, Novel antibifouling nanofiltration polyethersulfone membrane fabricated from embedding TiO_2 coated multiwalled carbon nanotubes, Sep. Purif. Technol., 90 (2012) 69–82.
[26] L.J. Zhu, L.P. Zhu, L.H. Jiang, Z. Yi, Y.F. Zhao, B.K. Zhu, Y.Y. Xu, Hydrophilic and antifouling polyethersulfone ultrafiltration membranes with poly(2-hydroxyethylmethacrylate) grafted silica nanoparticles as additive, J. Membr. Sci., 451 (2014) 157–168.
[27] Z.F. Fan, Z. Wang, N. Sun, J.X. Wang, S.C. Wang, Performance improvement of polysulfone ultrafiltration membrane by blending with polyaniline nanofibers, J. Membr. Sci., 320 (2008) 363–371.
[28] L. Wang, B.C. Benicewicz, Synthesis and characterization of dye-labeled poly(methacrylic acid) grafted silica nanoparticles, ACS Macro Lett., 2 (2013) 173–176.
[29] T.H. Young, L.W. Chen, Pore formation mechanism of membranes from phase inversion process, Desalination, 103 (1995) 233–247.
[30] V. Vatanpour, S.S. Madaeni, L. Rajabi, S. Zinadini, A.A. Derakhshan, Boehmite nanoparticles as a new nanofiller for preparation of antifouling mixed matrix membranes, J. Membr. Sci., 401–402 (2012) 132–143.
[31] G.L. Zhang, S.F. Lu, L. Zhang, Q. Meng, C. Shen, J.W. Zhang, Novel polysulfone hybrid ultrafiltration membrane prepared with TiO_2-g-HEMA and its antifouling characteristics, J. Membr. Sci., 436 (2013) 163–173.
[32] X.F. Wang, X.M. Chen, K. Yoon, D.F. Fang, B.S. Hsiao, B. Chu, High flux filtration medium based on nanofibrous substrate with hydrophilic nanocomposite coating, Environ. Sci. Technol., 39 (2005) 7684–7691.
[33] Y.F. Li, Y.L. Su, X.T. Zhao, X. He, R.N. Zhang, J.J. Zhao, X.C. Fan, Z.Y. Jiang, Antifouling, high-flux nanofiltration membranes enabled by dual functional polydopamine, ACS Appl. Mater. Interfaces, 6 (2014) 5548–5557.
[34] J. Yin, M. Chen, X.A. Cai, Preparation of polyethersulfone composite ultrafiltration membrane and its oil/water separation performance, J. Chin. Ceram. Soc., 4 (2020) 558–566.